Available online at www.sciencedirect.com

ScienceDirect

Ceramics International 40 (2014) 1481–1488

CERAMICS INTERNATIONAL

www.elsevier.com/locate/ceramint

Synthesis of silicon carbide whiskers using reactive graphite as template

Yawei Li[a], Qinghu Wang[a,*], Haibing Fan[b], Shaobai Sang[a], Yuanbing Li[a], Lei Zhao[a]

[a]The Hubei Province Key Laboratory of Ceramics and Refractories, Wuhan University of Science & Technology, Wuhan 430081, PR China
[b]Wuhan Research Institute of Metallurgical Construction, China Metallurgical Group Co., Ltd., Wuhan 430081, PR China

Received 15 June 2013; received in revised form 5 July 2013; accepted 5 July 2013
Available online 11 July 2013

Abstract

Silicon carbide whiskers have been synthesized by using reactive graphite as a template. Natural graphite flake was firstly activated using chemical oxidation and thermal oxidation methods. After that, the reactive graphite sources were mixed with silicon powder and heated in the coke bed at 1200 and 1400 °C. The structural evolution of graphite and morphologies of SiC whiskers were studied with the aids of XRD, SEM, TEM and EDS techniques. The results showed that natural graphite flake can be activated into reactive graphite such as oxidized graphite and expanded graphite with much more defects using thermal and chemical oxidation methods. The expanded graphite with a great deal of defects has higher reactivity than natural graphite flake and oxidized graphite and accelerates the formation of long and thick SiC whiskers. It is proposed that the vapor–solid mechanism is predominant for the growth of β-SiC whiskers in this system. During heating-up, Si or SiO vapors meet with the activated carbon atoms on graphite substrate to form SiC nucleus. Then these vapors continually deposit on the SiC nucleus following the SiC whiskers which grow along the ⟨111⟩ direction.
© 2013 Elsevier Ltd and Techna Group S.r.l. All rights reserved.

Keywords: Silicon carbide; Graphite flake; Expanded graphite

1. Introduction

In the past decades, much attention has been paid to silicon carbide (SiC) whiskers due to their excellent properties, such as high hardness, good flexibility, high thermal conductivity, high thermal stability and large band gap [1–3]. Consequently, they are widely used to fabricate structural and functional composites for extremely harsh environment [4,5]. Nowadays, various synthesis methods have been explored to produce β-SiC whiskers, including chemical vapor deposition using silicon precursor [6–8], carbon template of carbon nanotubes to β-SiC whiskers [9,10], thermal evaporation [11,12], carbothermal reduction [13], etc. Generally, the growth mechanisms of SiC whiskers are involved in vapor–solid (VS) and vapor–liquid–solid (VLS) mechanisms [14–17]. As for VS mechanism, Si-containing vapors such as Si (g) or SiO (g) react with CO (g) or C (s) to form SiC nucleus and the whiskers or nanowires grow along the directions of the least stable plane. In the VLS mechanism, once SiC nucleus formed, the metal droplets on the nucleus absorb Si (g) and SiO (g) gaseous species and the SiC whiskers precipitate from supersaturated liquid at the liquid–solid interface. Based on the mechanisms mentioned above, carbon source is very important in the process of preparing SiC whiskers. Until now, carbon nanotubes, carbon black, carbon fiber and phenolic resin, etc., were used to synthesize SiC whiskers [18–21]. The carbon source usually operates as reductant and substrate for the formation of SiC whiskers. Chen et al. [22] synthesized SiC nanowires on the substrate of polyacrylonitrile carbon fiber by evaporating silicon and proposed that Si-containing vapors are easily absorbed at points of flaws and react with the active carbon atoms quickly. Also, activated carbon was selected as carbon source to prepare SiC whiskers by many researchers [23–26]. However, most work focused on the morphologies of SiC whiskers, so it is still indistinct how the carbon sources impact on the growth of SiC whiskers. In our previous work, SiC whiskers preferentially appeared on the edge of graphite flake in Al_2O_3–C refractories, whereas silicon carbide granules grew in this system when using carbon black as carbon source [27]. It seems that the formation

*Corresponding author. Tel.: +86 27 68862188; fax: +86 27 68862018.
E-mail address: qhwang_material@126.com (Q. Wang).

0272-8842/$ - see front matter © 2013 Elsevier Ltd and Techna Group S.r.l. All rights reserved.
http://dx.doi.org/10.1016/j.ceramint.2013.07.032

of SiC whiskers was strongly dependent on the structure of graphite flake and related to the defects such as fractured C═C bonds at the edge of graphite, which are called as activated carbon atoms. So it was supposed that graphite flake acts as template and these defects existing on graphite can react with SiO (g) or Si (g) in order to nucleate SiC whiskers.

The objective of this work is to further elucidate the growth mechanism of SiC whiskers and to develop a novel method to synthesize SiC whiskers using reactive graphite as template. Natural graphite flake was firstly activated using thermal oxidation and chemical oxidation methods to prepare reactive graphite sources such as oxidized graphite and expanded graphite with much more defects than natural graphite flake. Then these kinds of graphite were mixed with silicon powder and heated in coke bed at 1200 and 1400 °C to prepare SiC whiskers based on the activated graphite templates.

2. Experimental

2.1. Preparation of the activated graphite

Two approaches have been used to activate graphite flake. To prepare the oxidized graphite, natural graphite flake (100 mesh, 97.58 wt% fixed carbon, China) was heat-treated in a sealed heat-resistant steel (cubiform reactor, 100 mm × 110 mm × 250 mm) at 1000 °C for 3 h. To prepare the expanded graphite, the same graphite flake was chemically oxidized by the Hummers method [28] and then exfoliated in a microwave oven for 20 s.

2.2. Fabrication of specimens

Three kinds of specimens were prepared by mixing silicon powder (45 μm, 98.47 wt% Si, Anyang Yuhong Metallurgy & Refractory Co., Ltd., China) with graphite flake, oxidized graphite and expanded graphite. The C/Si weight ratios of all specimens were 2:1. These mixtures were then cold pressed into cylindrical specimens with 20 mm in diameter and 20 mm in height at 30 MPa. The specimens containing graphite flake, oxidized graphite and expanded graphite were designated as GF, OG and EG, respectively.

All batches of specimens were placed inside a corundum sagger with a cover, which was filled with carbon black powder. Finally, the whole sagger was placed into an electrical furnace and heated from room temperature to 1200 °C and 1400 °C with a heating rate of 5 °C/min and a holding time of 3 h before cooling to room temperature.

2.3. Characterization and measurement methods

Thermogravimetry–differential scanning calorimetry (TG–DSC, STA499, NETZSCH, Germany) was employed to evaluate the reactivity and to calculate the non-isothermal oxidation kinetics of graphite flake, oxidized graphite and expanded graphite. Meanwhile, the Raman spectra of carbon sources were obtained with a high-resolution, dispersive Raman spectrometer system (Horiba-Jobin Yvon LabRam HR) equipped with a confocal microscope (Olympus BX-30) and a notch filter (532 nm). The phase compositions and microstructure of the specimens were analyzed by X-ray diffraction (XRD, X'Pert Pro, Philips, Netherlands), a scanning electron microscope (SEM, Quanta 400, FEI Company, USA) equipped with an energy dispersive X-ray spectroscope (EDS, Noran 623M-3SUT, Thermo Electron Corporation, Japan) and a high-resolution transmission electron microscope (HR-TEM, Model JEM-2010, JEOL, Japan).

3. Results and discussion

3.1. The structural characterization and reactivity of graphite

Fig. 1 shows the SEM micrographs of three kinds of graphite. It can be clearly seen that the natural graphite flake possesses relatively smooth basal planes and a few multilayer terraced edges with length of dozens of micrometers (Fig. 1a). Whereas, after thermal oxidation, much more multilayer terraced edges were observed on the surfaces of the oxidized graphite (Fig. 1b). It can be clearly seen that much more C═C bonds were broken on the basal planes. Interestingly, the expanded graphite showed a loose and worm-like structure, in which the basal layers were opened thoroughly to form large amount of pores.

Raman spectroscopy has been widely used to identify disorder of sp^2-network in different carbon sources [29–33]. The Raman signature at about 1585 cm^{-1} is known as the first-order of G band, which is the only feature in highly ordered crystalline graphite (e.g. HOPG, Highly Oriented Pyrolitic Graphite). The first-order of D band (D for disorder)

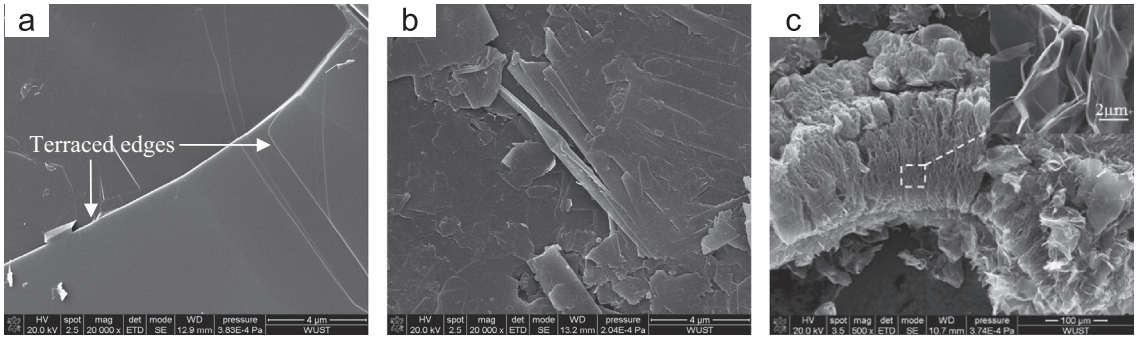

Fig. 1. SEM micrographs of (a) natural graphite flake, (b) oxidized graphite and (c) expanded graphite.

at about 1345 cm^{-1} is the characteristic feature of amorphous carbon materials containing sp^2 graphitic islands and disordered samples of graphite (e.g. nano-crystalline and micro-crystalline graphite). Therefore, Raman spectra of the graphite were measured to identify disorder of their crystalline structure (Fig. 2). For natural graphite flake, very strong G and D peaks are observed, indicating relatively intact lattice with few defects of graphite flake. By thermally oxidizing the graphite flake, the intensity of the G peak decreases and the intensity of the D peak increases, manifesting lattice damage occurred on the substrate of the oxidized graphite. Moreover, compared with graphite flake and oxidized graphite, the expanded graphite has the weakest G peak and the strongest D peak, demonstrating the existence of more defects on the substrate of the expanded graphite. The existence of defects in crystalline structure of carbon source leads to fractured C═C bonds, which are the source of activated carbon atoms. Actually, the crystalline structure is closely related to the reactivity of graphite.

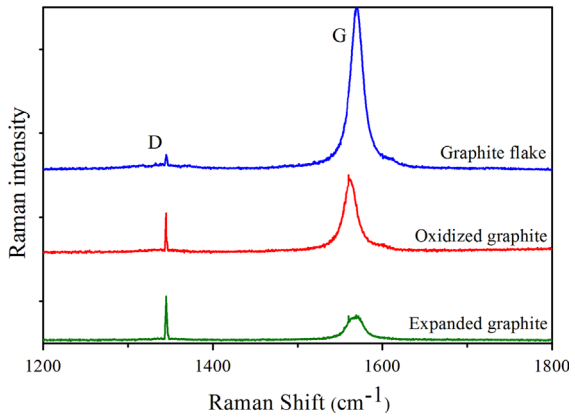

Fig. 2. Raman spectra of carbon sources.

The difference in the reactivity of different graphites may be revealed by their activation energies of oxidation. Both Kissinger's and Ozawa's methods for nanlysing non-isothermal kinetics were employed to estimate activation energies of oxidation for graphites in the present study [34–37]. Calorimetic signals of phase transformation were recorded in DSC analysis when the samples were continuously-heated from room temperature to 1200 °C in a static air atmosphere at different rates in the range of 5–20 °C/min. Fig. 3 shows the heating rate dependence of DSC curves for graphite flake, oxidized graphite and expanded graphite. The Kissinger and Ozawa plots for graphites are given in Fig. 4. The Kissinger method is based on Eq. (a), where T_{pi} is the peak temperature of the maximal mass loss rate, β_i is the heating rate, R is the gas constant. The model parameters A_k and E_k are the frequency factor and activation energy, respectively. The Ozawa plot is based on Eq. (b), where $G(a)$ is the integral energy of the reaction. Activation energy E_k can be obtained from the slopes of the straight lines for the functions, with $\ln(\beta_i/T_{pi}^2)$ vs. $1/T_{pi}$

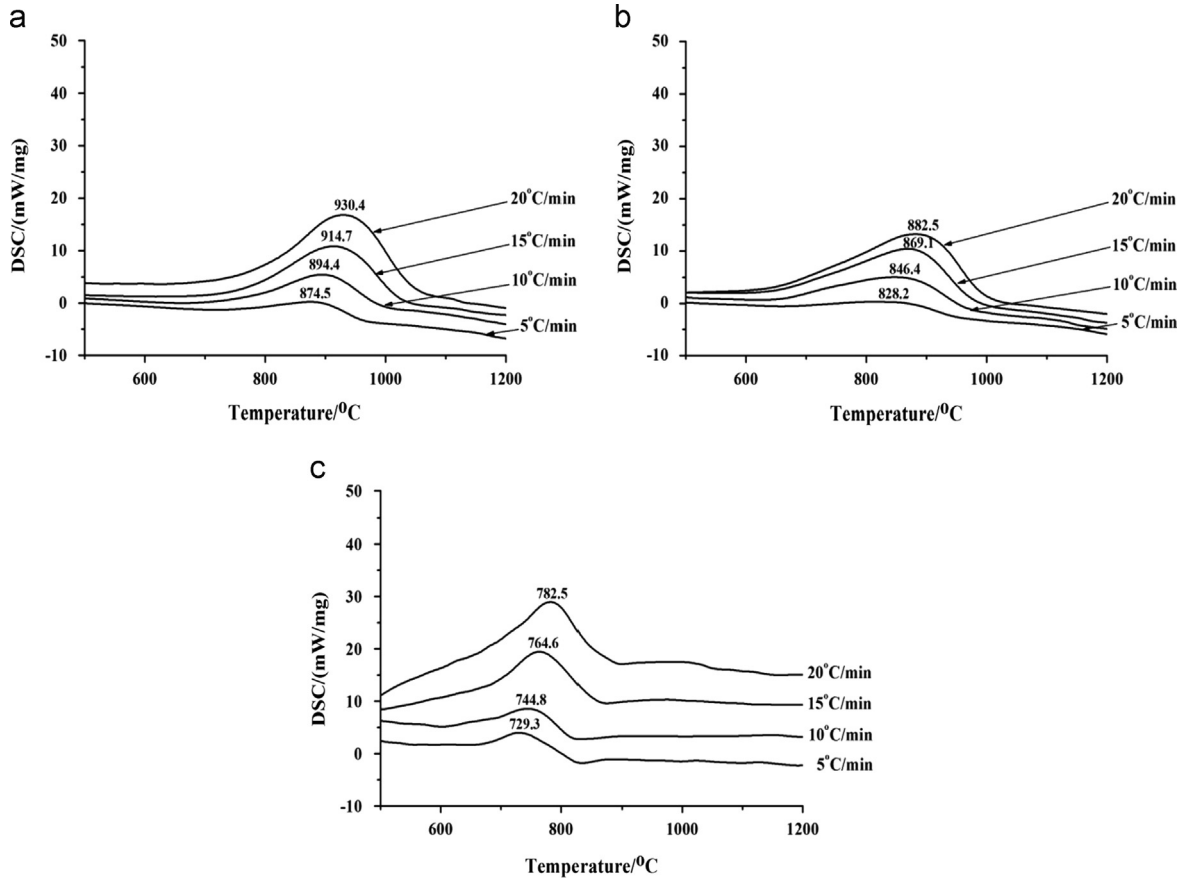

Fig. 3. Heating rate dependence of DSC curves for the oxidation of (a) graphite flake; (b) oxidized graphite; and (c) expanded graphite.

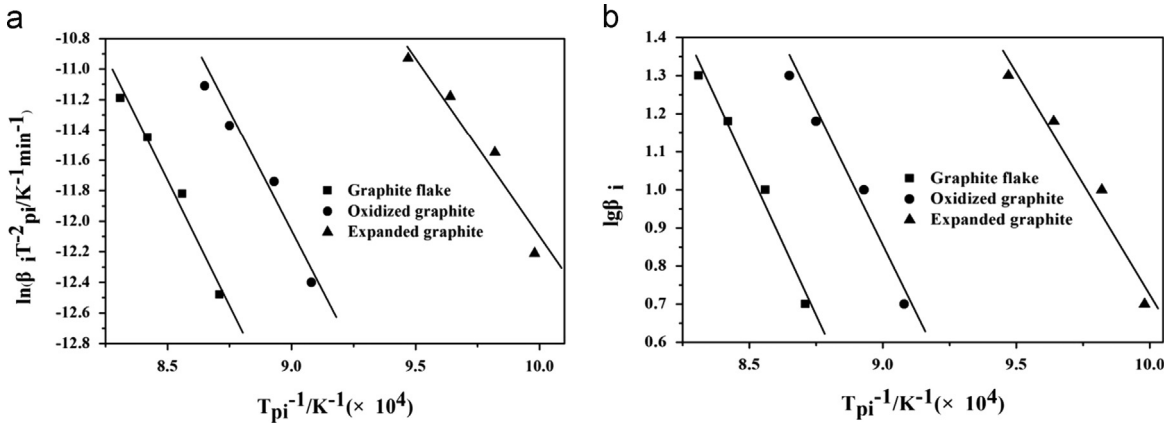

Fig. 4. Kissinger plots, $\ln(\beta i/T_{pi}^2)$ vs. $1/T_{pi}$ (a) and Ozawa plots, $\lg \beta i$ vs. $1/T_{pi}$(b) of graphite.

for the Kissinger method and $\lg \beta_i$ vs. $1/T_{pi}$ for the Ozawa method.

The oxidation activation energy calculated from the slopes of the Kissinger and Ozawa plots is almost the same to each graphite (Table 1). For example, the oxidation activation energies of graphite flake are 270.21 kJ/mol and 273.07 kJ/mol. However, each carbon source has specific oxidation activation energy. The oxidation activation energies of oxidized graphite are lower than those of graphite flake. Furthermore, the oxidation activation energies of expanded graphite are 221.98 kJ/mol and 218.34 kJ/mol, which are the lowest values among all the three carbon sources. So, it is supposed that oxidation activation energy is associated with the reactivity of carbon source. The lower oxidation activation energy indicates the higher reactivity, and represents the higher density of defects existing on the substrate of graphites.

$$\ln\left(\frac{\beta_i}{T_{pi}^2}\right) = \ln\frac{A_k R}{E_k} - \frac{E_k}{R}\frac{1}{T_{pi}} \quad (a)$$

$$\lg\beta_i = \lg\left(\frac{A_k E_k}{RG(a)}\right) - 2.315 - 0.4567\frac{E_k}{RT_{pi}} \quad (b)$$

3.2. The growth of SiC based on graphite

XRD patterns shown in Fig. 5 indicate the phase evolution of the specimens fired at 1200 and 1400 °C. For all the specimens fired at 1200 °C, not only very strong diffraction peaks of graphite and silicon, but also weak diffraction peaks of the β-SiC and the cristobalite were observed simultaneously (Fig. 5a). Up to 1400 °C, the silicon phase disappears and the β-SiC amount increases (Fig. 5b). Such phase evolution in specimens can be predicted by phase stability regions in Si–C–O–N diagram [38].

However, the reactivity of graphite made an impact on the phase evolution progress in the specimens. The highest diffraction peaks of the β-SiC (Fig. 5a and b) are observed in specimen EG followed by those in specimen GF and OG, manifesting that silicon was consumed and more β-SiC formed in the specimen EG. The peaks around $2\theta = 35.6°$, 41.4°, 60.0° and 71.8° correspond to (111), (200), (220) and (311) planes of cubic SiC [39,40], respectively. Moreover, some weak diffraction peaks of cristobalite were still observed in specimen GF fired at 1400 °C, which is attributed to the lower reactivity of graphite flake compared with those of the oxidized graphite and the expanded graphite.

Table 1
The oxidation activation energies (kJ/mol) of graphite flake, oxidized graphite and expanded graphite in air.

Methods	Graphite flake	Oxidized graphite	Expanded graphite
Kissinger	270.21	260.23	221.98
Ozawa	273.07	258.50	218.34

The SEM micrographs of all the specimens fired at 1200 °C are shown in Fig. 6. For the specimen GF with graphite flake as a carbon source, a spot of fine and short SiC whiskers with curved morphology formed on the edge of lamellar graphite randomly (Fig. 6a) and left some micropores on the lamellar graphite. As for the specimen OG, a few graphite and large amount of fine and short SiC whiskers which interlaced with each other were observed on the surface of the oxidized graphite (Fig. 6b). The most interesting phenomenon is observed in the specimen with expanded graphite as a carbon source. Although the overall appearance retained the lamella morphology of expanded graphite, large amount of SiC whiskers knitted with each other to form a network structure (Fig. 6c). In addition, some whiskers in specimen EG are longer and thicker in comparison with those in specimens GF and OG.

Fig. 7 shows the SEM micrographs of all the specimens fired at 1400 °C. Compared to the specimens fired at 1200 °C, much more whiskers grew at the expense of structural evolution and gradual disintegration of carbon source. For example, more fine and short SiC whiskers begin to encroach on graphite flake substrate, resulting in residual islet-like graphite (Fig. 7a) in the specimen GF fired at 1400 °C. The substrates of the oxidized graphite and the expanded graphite are encroached completely by large amount of SiC whiskers which interlock with each other to form intertextures in the

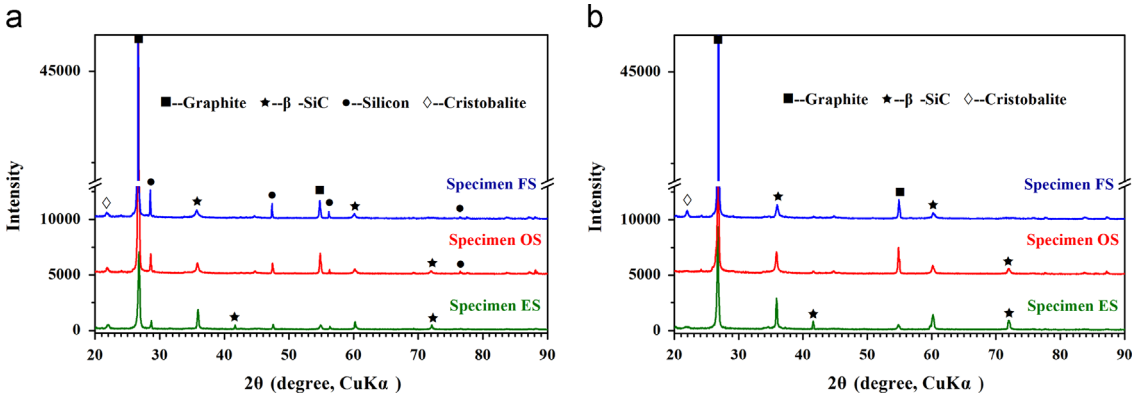

Fig. 5. XRD patterns of the specimens fired at (a) 1200 °C and (b) 1400 °C.

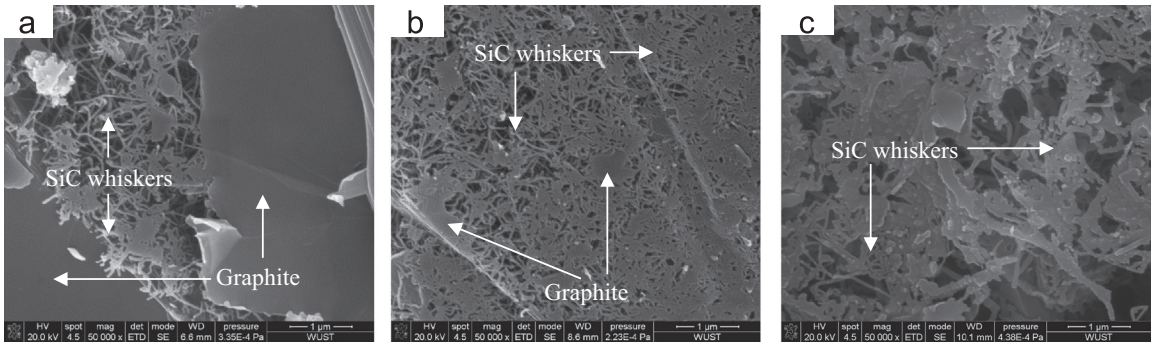

Fig. 6. SEM micrographs of the ruptured specimens (a) GF, (b) OG and (c) EG fired at 1200 °C.

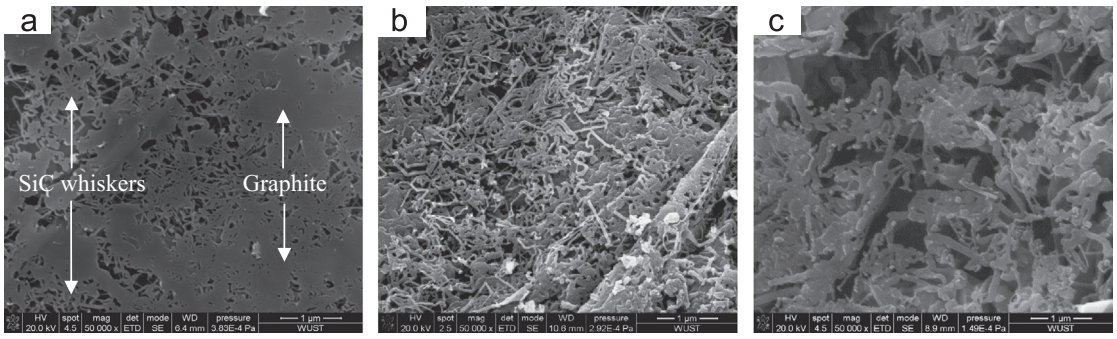

Fig. 7. SEM micrographs of the ruptured specimens (a) GF, (b) OG and (c) EG fired at 1400 °C.

specimen OG (Fig. 7b) and EG (Fig. 7c) fired at 1400 °C. Moreover, much more thick SiC whiskers were observed in specimen EG (Fig. 7c).

Fig. 8 shows the TEM micrographs of the SiC whiskers in the specimen GF fired at 1400 °C. A large amount of SiC whiskers extend outward from the edge of a graphite flake (Fig. 8a). According to Fig. 8b, most of the SiC whiskers are wire-like and have a diameter ranging from 15 to 40 nm and length up to several microns. No metallic droplets can be found at the tips of SiC whiskers. This means that the VS mechanism is responsible for the growth of SiC whiskers [22]. Fig. 8c shows the HR-TEM micrographs of an individual SiC whisker. The crystal lattice spacing is measured to be 0.25 nm, which is consistent with that of the (111) plane space of β-SiC crystal [41]. It is clearly seen that SiC whiskers grow along the direction normal to the (111) plane. This can be interpreted that the axis is preferentially normal to the lowest surface energy plane, which is the (111) plane for β-SiC crystallographic planes [42].

3.3. Discussion

Based on the results of XRD, SEM and TEM analysis, the growth of SiC whiskers depends strongly on gaseous phases, such as Si (g) and SiO (g) and the reactivity of graphite. The possible gaseous phases in Si–O–C system at high temperature can be predicted by thermodynamic calculation with Equilib module in FACT Sage package during heating-up [43]. The atmosphere in carbon black bed to fire all the specimens is approximately 0.35 atm CO and 0.65 atm N_2 [44]. Moreover, 33.3 g Si and 66.7 g C were the batch composition of

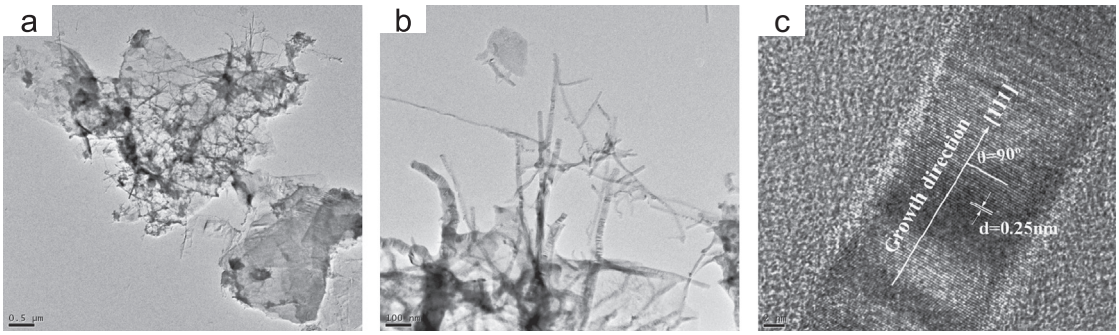

Fig. 8. Low (a, b) and high (c) magnification TEM micrographs of SiC whiskers.

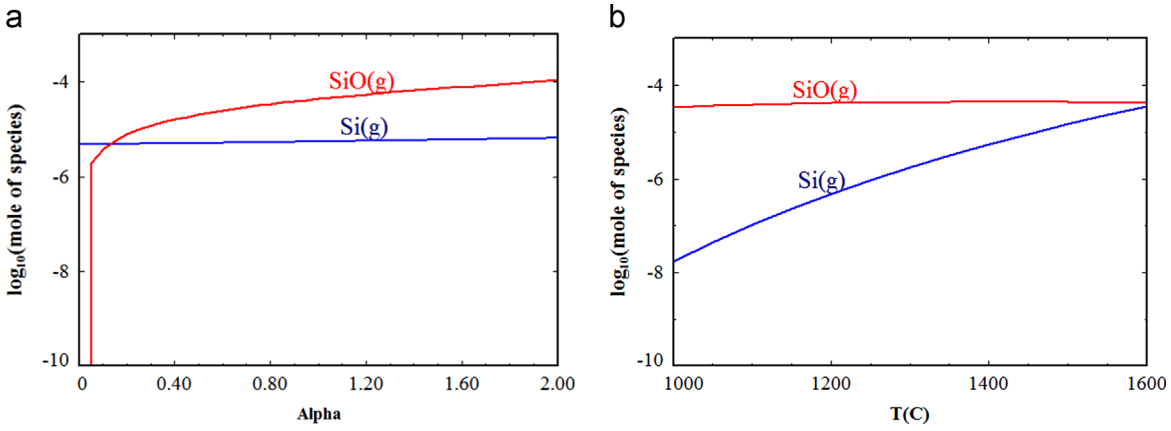

Fig. 9. Composition of Si-containing vapors (a) depending of Alpha for 1400 °C and (b) depending on the temperature for Alpha=1.

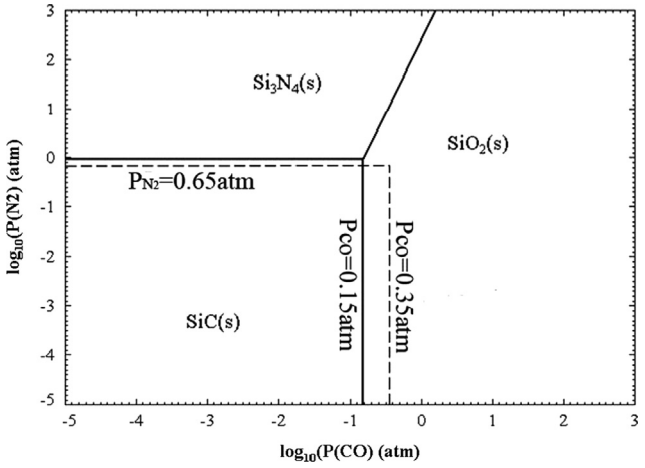

Fig. 10. Predominance area diagrams of the system Si–C–O–N at 1400 °C.

specimens for the calculations. Alpha is the weight ratio of the atmosphere and material [45] in the system.

Fig. 9(a) reveals that SiO (g) will be produced together with Si (g) once CO (g) is introduced in the environment at 1400 °C. Also the partial pressure of SiO (g) increases and surpasses the partial pressure of Si (g) with the increase of Alpha value. In a word, SiO (g) is the predominant gaseous species in the Si–O–C–N system, whereas the partial pressure of Si (g) increases with the increase of temperature when Alpha=1 (Fig. 9(b)). The gaseous Si (g) and SiO (g) come from the evaporation and oxidation of silicon via Reactions (1), (2) or (3) at high temperatures [46].

$$Si(s) = Si(g) \quad (1)$$

$$2Si(s) + O_2(g) = 2SiO(g) \quad (2)$$

$$Si(s) + CO(g) = SiO(g) + C(s) \quad (3)$$

The predominance area diagram for the Si–C–O–N system at 1400 °C is depicted in Fig. 10. It is revealed that the SiC is the stable phase when the partial pressures of N_2 and CO are lower than 0.65 atm and 0.15 atm, respectively. However, the SiO_2 would form when the partial pressure of CO is larger than 0.15 atm. Both the formation of the SiO according to Reaction (3) and also of SiO_2 in the closed system from CO and Si reduce the partial pressure of CO until the composition lies within the SiC field. The above analysis is in accordance with results in the phase composition in Fig. 5.

With regard to reactivity of carbon source, in general, graphite flake maintains relatively intact lattice structure with a few carbon atoms with high reactivity at the multilayer terraced edges [47]. However, such structural integrity of graphite can be forfeited due to severe oxidation. Hahn [48] reported that thermal oxidation of graphite leads to the formation of shallow pits, which are believed to originate from the point defects in the basal plane. As lots of defects exist in the crystal structure of oxidized graphite, the fractured C=C bonds generated from heating-up of graphite flake. In addition, Shen et al. [49] found that the chemical oxidation of

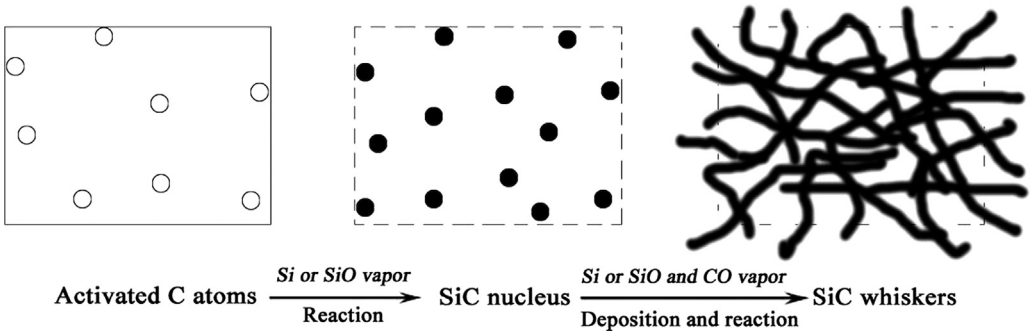

Fig. 11. Schematic of SiC whiskers grow on graphite substrate.

the carbon sources with acids introduces considerable oxygen-containing functional groups onto the layers, and even breaks the skeleton C=C bonds, thus leaving carbon fragments with dangling bonds on the edges. Therefore, much larger density of defects exists in the plane of expanded graphite, which underwent chemical oxidation.

Combining with phase composition and reactivity of graphite, the reaction process for growth of SiC whiskers is proposed as following stages. Firstly, Si (g) or SiO (g) vapors migrate by diffusive mass transfer at high temperature within this system. Secondly, when these gaseous species meet with the activated carbon atoms, the SiC nucleus would be formed according to the VS process [Reactions (4) and (5)]. Finally, after the nucleation of SiC, Si (g) or SiO (g) vapors deposit on the SiC nucleus continually, the SiC whiskers will be initially formed on the surface of the carbon source [Reactions (6) and (7)]. For instance, the natural graphite flake possesses relatively intact lattice structure and most of the fractured C=C bonds exist on the terraced edges of substrate. Consequently, SiC whiskers formed preferentially on the terraced edges of lamellar graphite in the specimen GF fired at 1200 °C (Fig. 6a). In comparison, the expanded graphite characterized by many defects possessed the highest reactivity and accelerated the growth of SiC whiskers in comparison with the other graphite types. The above mentioned evolutionary process from activated carbon atoms to SiC whiskers can be described in Fig. 11.

$$Si(g) + C(s) = SiC(nucleus) \quad (4)$$

$$SiO(g) + 2C(s) = SiC(nucleus) + CO(g) \quad (5)$$

$$2Si(g) + 2CO(g) = 2SiC(whiskers) + O_2(g) \quad (6)$$

$$SiO(g) + 3CO(g) = SiC(whiskers) + 2CO_2(g) \quad (7)$$

4. Conclusions

Natural graphite flake can be activated into reactive graphite with much more defects using thermal oxidation and chemical oxidation methods. The expanded graphite has higher density of defects and higher reactivity than natural graphite flake and oxidized graphite, and accelerates the formation of long and thick SiC whiskers. VS mechanism is predominant for the growth of β-SiC whiskers in this system. During heating-up, Si (g) or SiO (g) vapors meet with the activated carbon atoms on the graphite substrate and form SiC nucleus. Then these vapors continually deposit on the SiC nucleus following the SiC whiskers which grow along the ⟨111⟩ direction.

Acknowledgments

The authors thank the financial support from the Project-sponsored by SRF for ROCS, SEM (K01103), Natural Science Foundation of Hubei Province (2009CDA050), Natural Science Foundation of China (51072143) and Wuhan Science and Technology Bureau (2013010602010210).

References

[1] E.W. Wong, P.E. Sheehan, C.M. Lieber, Nanobeam mechanics: elasticity, strength, and toughness of nanorods and nanotubes, Science 277 (1997) 1971–1975.
[2] A.A. Lebedev, Heterojunctions and superlatices based on silicon carbide, Semiconductor Science and Technology 21 (2006) R17–R34.
[3] S. Ishihara, H. Tanaka, T. Nishimura, Synthesis of silicon carbide powder from fumed silica powder and phenolic resin, Journal of Materials Research 21 (2006) 1167.
[4] L.M. Shi, H.S. Zhao, Y.H. Yan, Z.Q. Li, C.H. Tang, Synthesis and characterization of submicron silicon carbide powders with silicon and phenolic resin, Powder Technology 169 (2006) 71–76.
[5] L. Yang, X. Zhang, R. Huang, G. Zhang, C. Xue, Formation of β-SiC nanowires by annealing SiC films in hydrogen atmosphere, Physica E 35 (2006) 146–150.
[6] W. Yang, H. Araki, A. Kohyama, S. Thaveethavorn, H. Suzuki, T. Noda, Fabrication in-situ SiC nanowires/SiC matrix composite by chemical vapour infiltration process, Materials Letters 58 (2004) 3145–3148.
[7] Y.H. Chu, Q.G. Fu, Z.Z. Zhang, H.J. Li, K.Z. Li, Q. Lei, Microstructure and growth mechanism of SiC nanowires with periodically fluctuating hexagonal prisms by CVD, Journal of Alloys and Compounds 508 (2010) L36–L39.
[8] J. Wei, K.Z. Li, J. Chen, H.D. Yuan, Synthesis of centimeter-scale ultra-long SiC nanowires by simple catalyst-free chemical vapor deposition, Journal of Crystal Growth 335 (2011) 160–164.
[9] C.C. Tang, S.S. Fan, H.Y. Dang, J.H. Zhao, C. Zhang, P. Li, et al., Growth of SiC nanorods prepared by carbon nanotubes-confined reaction, Journal of Crystal Growth 210 (2000) 595–599.
[10] Z.W. Pan, H.L. Lai, C.K. Au Frederick, X.F. Duan, W.Y. Zhou, W. S. Shi, et al., Oriented silicon carbide nanowires: synthesis and field emission properties, Advanced Materials 12 (2000) 1186–1190.
[11] C. Vix-Guterl, B. Mc-Enaney, P. Ehrburger, SiC material produced by carbothermal reduction of a freeze gel silica–carbon artifact, Journal of the European Ceramic Society 19 (1999) 427–432.

[12] W.M. Zhou, X. Liu, Y.F. Zhang, Simple approach to β-SiC nanowires: synthesis, optical, and electrical properties, Applied Physics Letters 89 (2006) 223124.
[13] G.W. Meng, L.D. Zhang, C.M. Mo, S.Y. Zhang., H.J. Li, Y. Qin, et al., Synthesis of one-dimensional nanostructures-β-SiC nanorods with and without amorphous SiO_2 wrapping layers, Metallurgical and Materials Transactions A 30 (1999) 213–219.
[14] R.S. Wagner, W.C. Ellis, Vapor–liquid–solid mechanism of single crystal growth, Applied Physics Letters 4 (1964) 89–90.
[15] S. Cetinkaya, S. Eroglu, Chemical vapor deposition of C on SiO_2 and subsequent carbothermal reduction for the synthesis of nanocrystalline SiC particles/whiskers, International Journal of Refractory Metals and Hard Materials 29 (2011) 566–572.
[16] Y.J. Hao, J.B. Wagner, D.S. Su, G.Q. Jin, X.Y. Guo, Beaded silicon carbide nanochains via carbothermal reduction of carbonaceous silica xerogel, Nanotechnology 17 (2006) 2870–2874.
[17] J. Wei, K.Z. Li, H.J. Li, Q.G. Fu, L. Zhang, Growth and morphology of one-dimensional SiC nanostructures without catalyst assistant, Materials Chemistry and Physics 95 (2006) 140–144.
[18] H.S. Zhao, L.M. Shi, Z.Q. Li, C.H. Tang, Silicon carbide nanowires synthesized with phenolic resin and silicon powders, Physica E 41 (2009) 753–756.
[19] Y.J. Wu, J.S. Wu, W. Qin, D. Xu, Z.X. Yang, Y.F. Zhang, Synthesis of β-SiC nanowhiskers by high temperature evaporation of solid reactants, Materials Letters 58 (2004) 2295–2298.
[20] R.V. Krishnarao, J. Subrahmanyam, Formation of SiC from rice husk silica–carbon black mixture: effect of rapid heating, Ceramics International 22 (1996) 489–492.
[21] F.P. Huang, H.J. Li, K.Z. Li, C.H. Wang, Prefabrication of SiC whiskers through induction of carbon fiber, Transactions of Nonferrous Metals Society of China 16 (2006) 483–487.
[22] J.J. Chen, R.B. Wu, G.Y. Yang, Y. Pan, J. Lin, L.L. Wu, et al., Synthesis and photoluminescence of needle-shaped 3C–SiC nanowires on the substrate of PAN carbon fiber, Journal of Alloys and Compounds 456 (2008) 320–323.
[23] J. Zhang, J.C. Jeong, J.H. Lee, C.W. Won, D.J. Kim, C.O. Kim, The effect of carbon sources and activative additive on the formation of SiC powder in combustion reaction, Materials Research Bulletin 37 (2002) 319–329.
[24] Y.H. Gao, Y. Bando, K. Kurashima, T. Sato, SiC nanorods prepared from SiO and activated carbon, Journal of Materials Science 37 (2002) 2023–2029.
[25] J. Wei, K.Z. Li, H.J. Li, H.B. Ouyang, Z.J. Li, C. Wang, Photoluminescence performance of SiC nanowires, whiskers and agglomerated nanoparticles synthesized from activated carbon, Physica E 41 (2009) 1616–1620.
[26] W.M. Zhou, Z.X. Yang, F. Zhu, Y.F. Zhang, SiC/SiO_2 nanocables and nanosprings synthesized by catalyst-free method, Physica E 31 (2006) 9–12.
[27] H.B. Fan, Y.W. Li, S.B. Sang, Microstructures and mechanical properties of Al_2O_3–C refractories with silicon additive using different carbon sources, microsilica or their combination as additive, Materials Science and Engineering A 528 (2011) 3177–3185.
[28] W.S. Hummers, R.E. Offeman, Preparation of graphitic oxide, Journal of the American Chemical Society (1958) 1339.
[29] M.M. Lucchese, F. Stavale, E.H. Martins Ferreira, C. Vilani, M.V. O. Moutinho, Rodrigo B. Capaz, C.A. Achete, et al., Quantifying ion-induced defects and Raman relaxation length in graphene, Carbon 48 (2010) 1592–1597.
[30] Y. Wang, D.C. Alsmeyer, R.L. Mccreery, Raman spectroscopy of carbon materials: structural basis of observed spectra, Chemistry Materials 2 (1990) 557–563.
[31] Chiara Castiglioni, Matteo Tommasini, Raman spectroscopy of disordered and nano-structured carbon materials: the molecular approach, Optica Pura Y Aplicada 40 (2007) 169–174.
[32] S. Reich, C. Thomsen, Raman spectroscopy of graphite, Philosophical Transactions of the Royal Society A 362 (2004) 2271–2278.
[33] A.C. Ferrari, J. Robertson, Interpretation of Raman spectra of disordered and amorphous carbon, Physical Review B 61 (2000) 14095–14106.
[34] E. Illekova, K. Csomorova, Kinetics of oxidation in various forms of carbon, Journal of Thermal Analysis and Calorimetry 80 (2005) 103–108.
[35] P.G. Boswell, On the calculation of activation energies using a modified Kissinger method, Journal of Thermal Analysis 18 (1980) 353–358.
[36] W.Z. Hu, S.L. Gao, F.Q. Zhao, Kinetics of Thermal Analysis, Science Press, Beijing, 2008.
[37] M.J. Starink, A new method for the derivation of activation energies from experiments performed at constant heating rate, Thermochimica Acta 288 (1996) 97–104.
[38] Y.W. Li, X.L. Chen, Y.B. Li, S.L. Jin, S. Ge, L. Zhao, et al., Effect of silicon addition on pore structure and thermal conductivity of fired carbon specimens, Naihuo Cailiao 42 (2008) 401–408.
[39] Z. Liu, W. Shen, W. Bu, H. Chen, Z. Hua, L. Zhang, et al., Low-temperature formation of nanocrystalline β-SiC with high surface area and mesoporosity via reaction of mesoporous carbon and silicon powder, Microporous and Mesoporous Materials 82 (2005) 137–145.
[40] G.Q. Jin, X.Y. Guo, Synthesis and characterization of mesoporous silicon carbide, Microporous and Mesoporous Materials 60 (2003) 207–212.
[41] G.Y. Li, X.D. Li, H. Wang, L. Liu, Ultra long SiC nanowires with fluctuating diameters synthesized in a polymer pyrolysis CVD route, Solid State Sciences 11 (2009) 2167–2172.
[42] D.H. Wang, D. Xu, Q. Wang, Y.J. Hao, G.Q. Jin, X.Y. Guo, et al., Periodically twinned SiC nanowires, Nanotechnology 19 (2008) 215602.
[43] ⟨www.factsage.com⟩.
[44] X.L. Chen, Y.B. Li, Y.W. Li, Carbothermic reduction synthesis of Ti(C, N) powder in the presence of molten salt, Ceramics International 34 (2008) 1253–1259.
[45] X.L. Chen, Y.W. Li, Y.B. Li, Effect of temperature on the properties and microstructures of carbon refractories for blast furnace (BF), Metallurgical and Materials Transactions A 40 (2009) 1675–1683.
[46] M. Luo, Y.W. Li, S.L. Jin, S.B. Sang, L. Zhao, Microstructural evolution and oxidation resistance of multi-walled carbon nanotubes in the presence of silicon powder, Journal of Materials Science and Technology 28 (2012) 599–607.
[47] W. Jiang, G. Nadeau, K. Zaghib, K. Kinoshita, Thermal analysis of the oxidation of natural graphite-effect of particle size, Thermochimica Acta 351 (2000) 85–93.
[48] J.R. Hahn, Kinetic study of graphite oxidation along two lattice derections, Carbon 43 (2005) 1506–1511.
[49] Y.X. Shen, L. Yan, H.H. Song, J. Yang, G. Yang, X.H. Chen, et al., A general strategy for the synthesis of carbon nanofibers from solid carbon materials, Angewandte Chemie International Edition 51 (2012) 12202–12205.